Structure, phase transitions and molecular dynamics of $[C(NH_2)_3]_3[M_2I_9]$, M = Sb, Bi

2008 J. Phys.: Condens. Matter 20 255221

(http://iopscience.iop.org/0953-8984/20/25/255221)

J. Phys.: Condens. Matter **20** (2008) 255221 (12pp) doi:10.1088/0953-8984/20/25/255221

Structure, phase transitions and molecular dynamics of $[C(NH_2)_3]_3[M_2I_9]$, M = Sb, Bi

P Szklarz[1,4], A Pietraszko[2], R Jakubas[1], G Bator[1], P Zieliński[3] and M Gałązka[3]

[1] Faculty of Chemistry, University of Wrocław, Joliot–Curie 14, 50-383 Wrocław, Poland
[2] Institute of Low Temperature and Structure Research, PAS, Okólna 2, 50-950 Wrocław 2, PO Box 937, Poland
[3] The H Niewodniczański Institute of Nuclear Physics PAS, Radzikowskiego 152, PL-31-342 Kraków, Poland

E-mail: pszklarz@eto.wchuwr.pl

Received 3 March 2008, in final form 28 April 2008
Published 21 May 2008
Online at stacks.iop.org/JPhysCM/20/255221

Abstract

Two novel guanidinium iodoantimonate(III) and iodobismuthate(III) crystals, $[C(NH_2)_3]_3[Sb_2I_9]$ and $[C(NH_2)_3]_3[Bi_2I_9]$, have been synthesized and their structures have been determined by means of single-crystal x-ray diffraction studies at three temperatures (293, 348 and 362 K). Both compounds appeared to be isomorphous in corresponding phases. The crystal structure of the title compounds is composed of discrete $M_2I_9^{3-}$ (M = Sb, Bi) anions and $C(NH_2)^{3+}$ guanidinium cations. A non-equivalence of two guanidinium cations has been found. Both guanidinium analogs exhibit a rich sequence of phase transitions. In $Gu_3Sb_2I_9$, three solid–solid structural phase transformations of the first order type are detected at 119/121, 341/344 and 355/362 K (on cooling/heating) by the DSC and dilatometric techniques. $Gu_3Bi_2I_9$ displays four first order phase transitions: 179/185, 202/215, 287/291 and 358/368 K. The low temperature phases appear to have ferroic (ferroelastic) properties. The prototypic paraelastic phase for both compounds belongs to hexagonal symmetry (space group $P6_3/mmc$). The dielectric response has been measured in a wide frequency region (100 Hz–1 MHz), but no dielectric dispersion has been detected. Possible mechanisms of the phase transitions in $Gu_3M_2I_9$ (M = Sb, Bi) are discussed on the basis of the presented results.

(Some figures in this article are in colour only in the electronic version)

1. Introduction

The family of halogenoantimonates(III) and halogenobismuthates(III) of the general formula $R_aM_bX_{(3b+a)}$ (where R denotes the organic cation, M denotes metal Sb(III) or Bi(III) and X denotes halogen atom, Cl, Br, I) presents a group of interesting materials. Among these compounds, several crystals exhibiting nonlinear optical and electric properties have been found. These compounds are widely investigated due to possible modification of their physical properties by incorporation of various organic cations into the crystal structure. The cations to be incorporated into the structure should be small in size and bestow a non-symmetric charge distribution. The organic cations which give the best results in this sense are monomethyl, dimethyl and trimethylammonium ones as well as the aromatic cations like pyridinium and substituted pyridinium ones. Interesting results have also been obtained for compounds with guanidinium cations incorporated into the structure. It is well known that the guanidinium cation, being symmetric as a free molecule, is distorted in the crystal lattice, and in this way its dynamics may give a contribution to the electric polarization of crystals. It should be noted that among the $R_aM_bX_{(3b+a)}$ molecular–ionic salts several ferroelectrics have been discovered. The majority of these ferroelectric salts crystallize with the $R_3M_2X_9$ [1–6] or $R_5M_2X_{11}$

[4] Author to whom any correspondence should be addressed.

chemical composition [7–10]. Four forms of the anionic sublattice may be distinguished in the group of the $R_3M_2X_9$ salts: (i) two-dimensional layer structure, (ii) infinite one-dimensional chains, (iii) discrete bioctahedral units or (iv) tetraoctahedral units [3]. The ferroelectric properties of the $R_3M_2X_9$ type compounds are limited to the species characterized by the two-dimensional anionic substructure. The anionic framework of the other subclass of the halogenobismuthates(III), $R_5Bi_2X_{11}$, is built up exclusively of discrete bioctahedral units, $Bi_2X_{11}^{5-}$. All salts known so far and crystallizing with this stoichiometry possess ferroelectric properties [11]. The origin of the ferroelectricity of either the $R_3M_2X_9$ or $R_3M_2X_9$ subclass is ascribed to the orientational disorder of dipolar organic cations as well as to the large electric polarizability of the anionic sublattice. The guanidinium halogenoantimonates(III) and halogenobismuthates(III) synthesized so far were found to crystallize with three different chemical compositions: R_2MX_5, $R_3M_2X_9$ and R_3MX_6 [12–14]. Among them the compound characterized by the separated bioctahedral units $M_2X_9^{3-}$, namely $Gu_3Bi_2Br_9$ [15], appears to be the most interesting one. In the solid state this compound exhibits various polymorphic phase transitions and ferroic (ferroelastic) properties. It seems interesting to extend the study on the other guanidinium salts to check how the replacement of chlorine or bromine atoms by iodine ones modifies the structural and ferroic properties. In this paper the results of studies on the structure and thermal properties, dilatometric and differential scanning calorimetry (DSC) of the guanidinium analogs, $Gu_3Sb_2I_9$ and $Gu_3Bi_2I_9$, are described. The possible mechanisms of the phase transitions in the $Gu_3Sb_2I_9$ and $Gu_3Bi_2I_9$ compounds are discussed.

2. Experimental details

Crystals of the title compounds were grown by a slow evaporation of a concentrated HI solution containing the 3:2 ratio of $[C(NH_2)_3]_2CO_3$ and Sb_2O_3/Bi_2O_3. The salts obtained were twice re-crystallized and their composition was verified by an elemental analysis. The single crystals were grown from an aqueous solution at constant room temperature.

Differential scanning calorimetry (DSC) runs were recorded using a Perkin Elmer DSC-7 in the temperature range 100–470 K with a scanning rate 10 K min^{-1}. The TGA measurements were performed on a Setaram SETSYS 16/18 instrument in the temperature range 300–850 K with a ramp rate of 2 K min^{-1}. The scan was performed in flowing nitrogen (flow rate: 1 dm^3 h^{-1}). The dilatometric measurements were performed by a Perkin Elmer TMA-7 thermomechanical analyzer in the temperature range 140–300 K. The dimensions of the sample were of the order of $5 \times 3 \times 1$ mm^3. The temperature scanning rate was equal to 2 K min^{-1}.

The complex dielectric permittivity $\epsilon^* = \epsilon' - i\epsilon''$ was measured using an Agilent 4284A Precision *LCR* meter in the frequency range between 100 Hz and 1 MHz and in the temperature range from 90 to 400 K. The dimensions of the sample were of the order of $3 \times 3 \times 0.8$ mm^3. The overall error in estimation of the real and imaginary parts of the complex dielectric permittivity value was less than 5% and 10%, respectively.

The x-ray diffraction data were collected on a KUMA KM4CCD diffractometer equipped with graphite monochromated Mo Kα radiation and an Oxford Cryosystem cooling device. The crystal structures were solved by direct methods with the *SHELXS97* program and refined by a full-matrix least-squares method on all F^2 data using the *SHELXL97* program [18, 19]. All the heavy atoms were refined with anisotropic temperature factors. The H atoms were located from the molecular geometry and their isotropic temperature factors U_{iso} were assumed as 1.2 times U_{eq} of their closest heavy atoms. The crystal data together with experimental and refinement details are given in table 1. CrysAlis software (Oxford Diffraction Company) was used in data collection, cell refinement and data reduction processes [16, 17]. Crystallographic data for the structures reported in this paper have been deposited with the Cambridge Crystallographic Data Centre, CCDC no 678440, 678441, 678442, 678443 and 678444. Copies of this information may be obtained free of charge from the Director, CCDC, 12 Union Road, Cambridge CB2 1EZ, UK (fax, +44-1223-336033; e-mail, deposit@ccdc.cam.ac.uk, or http://www.ccdc.cam.ac.uk).

3. Results

3.1. Thermal properties (TGA, DTA, DSC and dilatometric)

The thermal stability of both iodide analogs was studied by means of simultaneous thermogravimetric analysis (TGA) and differential thermal analysis (DTA) scans between 320 and 850 K. These results, presented in figures 1(a) and (b), show that $Gu_3Bi_2I_9$ exhibits one endothermic peak at about 363 K on the DTA curve. The crystal seems to be stable up to about 590–600 K; above this temperature range a loss of weight exceeds 3%, which is treated as a limit of thermal stability of the compound. Further heating above 600 K leads to a melting of the sample, which is accompanied by onset of a continuous decomposition of the $Gu_3Bi_2I_9$ sample. The thermal properties of the antimony analog $Gu_3Sb_2I_9$ are more complex. On the DTA curve at least three endothermic peaks are displayed up to 460 K: at 340, 357 and 425 K. The fourth endothermic peak, found at 448 K, is probably connected with the fact that above 440–450 K an onset of the partial decomposition of $Gu_3Sb_2I_9$ takes place. A rapid decomposition of the sample is clearly seen at about 530–540 K, and above 630 K the $Gu_3Sb_2I_9$ compound is fully decomposed.

The results of the calorimetric measurements for $Gu_3Sb_2I_9$ and $Gu_3Bi_2I_9$ are illustrated in figures 2(a) and (b). When the $Gu_3Sb_2I_9$ sample is heated from room temperature up to 370 K two reversible heat anomalies at 344/341 and 362/355 K (on heating/cooling) are detected. These anomalies exhibit the features typical of the first order phase transition—a well shaped peak on the DSC curve and temperature hysteresis. The values of the entropy effect, ΔS, are equal to 19.1 and 15.4 J mol^{-1} K^{-1} for the 344 and 362 K transitions, respectively. On cooling of the $Gu_3Sb_2I_9$ sample below room temperature, one additional phase transition is

Table 1. Crystal data and structure refinement for $[C(NH_2)_3]_3[Sb_2I_9]$ (phases I, II and III) and $[C(NH_2)_3]_3[Bi_2I_9]$ (phase II).

	Phase III	Phase II	Phase I	Phase II
		Crystal data		
Empirical formula	$C_3H_{18}Sb_2I_9N_9$	$C_3H_{18}Sb_2I_9N_9$	$C_3H_{18}Sb_2I_9N_9$	$C_3H_{18}Bi_2I_9N_9$
Formula weight (g mol^{-1})	1565.86	1565.86	1565.86	1740.32
Crystal system, space group	Orthorhombic, $Cmcm$	Orthorhombic, $Cmcm$	Hexagonal, $P6_3/mmc$	Orthorhombic, $Cmcm$
a (Å)	11.108(2)	10.002(2)	9.2400(13)	10.5965(18)
b (Å)	13.364(3)	15.009(3)	9.2400(13)	14.0961(19)
c (Å)	20.878(6)	21.115(6)	21.760(4)	21.157(3)
V (Å^3)	3099.2(12)	3169.6(13)	1608.9(5)	3160.2(8)
Z	4	4	2	4
D_{calc} (g cm^{-3})	3.356	3.281	3.232	3.658
μ (mm^{-1})	10.717	10.479	10.322	19.922
F (000)	2712	2712	1356	2968
Crystal size (mm^3)	0.26 × 0.21 × 0.16	0.26 × 0.21 × 0.16	0.26 × 0.21 × 0.16	0.27 × 0.23 × 0.21
Crystal habit	Plate	Plate	Plate	Plate
		Data collection		
Diffractometer	Kuma KM4CCD	Kuma KM4CCD	Kuma KM4CCD	Kuma KM4CCD
Monochromator	Graphite	Graphite	Graphite	Graphite
Radiation type, wavelength, λ (Å)	Mo Kα, 0.710 73	Mo Kα, 0.710 73	Mo Kα, 0.710 73	Mo Kα, 0.710 73
T (K)	293(2)	348(2)	364(2)	293(2)
θ range (deg.)	4.16–33.14	3.79–24.40	4.41–24.70	4.09–28.28
Ranges of h, k, l	$-17 \leqslant h \leqslant 17$ $-14 \leqslant k \leqslant 20$ $-32 \leqslant l \leqslant 27$	$-11 \leqslant h \leqslant 11$ $-13 \leqslant k \leqslant 17$ $-24 \leqslant l \leqslant 24$	$-10 \leqslant h \leqslant 10$ $-10 \leqslant k \leqslant 10$ $-25 \leqslant l \leqslant 25$	$-13 \leqslant h \leqslant 14$ $-18 \leqslant k \leqslant 18$ $-27 \leqslant l \leqslant 27$
Absorption correction	Numerical	Numerical	Numerical	Numerical
T_{min}/T_{max}	0.3066/0.1050	0.2767/0.1012	0.3368/0.1334	0.2180/0.0438
Measured reflections	21 158	12 540	12 364	17 955
Independent reflections	3472	1428	566	2097
Observed refl. ($I > 2\sigma(I)$)				
R_{int}	0.0593	0.1063	0.2341	0.1076
		Refinement		
Refinement on	F^2	F^2	F^2	F^2
Data/restraints/parameters	3056/0/68	1428/5/68	566/2/30	2097/4/68
$R(F_0^2 > 2\sigma(F_0^2))$	$R_1 = 0.0492$ $wR_2 = 0.1134$	$R_1 = 0.0677$ $wR_2 = 0.1677$	$R_1 = 0.1533$ $wR_2 = 0.3247$	$R_1 = 0.0385$ $wR_2 = 0.0676$
R (all data)	$R_1 = 0.1038$ $wR_2 = 0.1265$	$R_1 = 0.1156$ $wR_2 = 0.1835$	$R_1 = 0.2533$ $wR_2 = 0.3621$	$R_1 = 0.1216$ $wR_2 = 0.0737$
$GooF = S$	1.087	1.655	2.124	0.821
Extinction	0.000 10(2)	0.000 121(4)	0.000 11(15)	0.000 125(8)
$\Delta\rho_{max}/\Delta\rho_{min}$ (e Å^{-3})	1.186/−1.184	1.022/−0.780	1.378/−0.629	1.141/−1.037

$w = 1/[\sigma^2(F_0^2) + (aP)^2 + bP]$ where $P = (F_0^2 + 2F_c^2)/3$.

found at 119/121 K on cooling/heating. The entropy effect, equal to 12.2 J mol^{-1} K^{-1}, is comparable with $R\ln 4 = 11.53$ J mol^{-1} K^{-1}. The high temperature phase is denoted as I and subsequently the phase below 355 K is denoted as II, below 341 K as III and below 119 K as IV. The situation for $Gu_3Bi_2I_9$ is more complex. When the crystal is cooled from room temperature (300 K) for the first time (scan c1) three reversible phase transitions have been detected at 287, 202 and 179 K (ΔS equal to 6.2, 4.4 and 9.5 J mol^{-1} K^{-1}, respectively). On a subsequent heating (scan h1) the corresponding phase transitions appear at 291, 215 and 185.6 K (ΔS equal to 5.7, 4.2 and 8 J mol^{-1} K^{-1}, respectively). In the heating scan h2 of the sample above room temperature a strong phase transition appears at about 368 K ($\Delta S = 17.7$ J mol^{-1} K^{-1}). This phase transition is well reversible (on cooling at 358 K). It should be noted that heating of the sample of $Gu_3Bi_2I_9$ above 370 K causes all the phase transitions below room temperature to have some tendency to be smeared (see scans c3 and h3). We should also add that all phase transitions found in $Gu_3Bi_2I_9$ are clearly of first order.

Figures 3(a) and (b) show the results of the linear thermal expansion, $\Delta L/L_0$, obtained along the [001], [$\bar{1}$10] and [$\bar{1}\bar{1}$0] directions (notation for the orthorhombic system) for the $Gu_3Sb_2I_9$ and $Gu_3Bi_2I_9$ samples. We show runs obtained during heating of the samples. We can state that dilatometric results are well consistent with the data obtained in the DSC measurements. The transformation at 344/341 K in $Gu_3Sb_2I_9$ is accompanied by the $\Delta L/L_0$ change characteristic of a discontinuous transformation. The anomaly in $\Delta L/L_0$ corresponding to the phase transition is observed during the

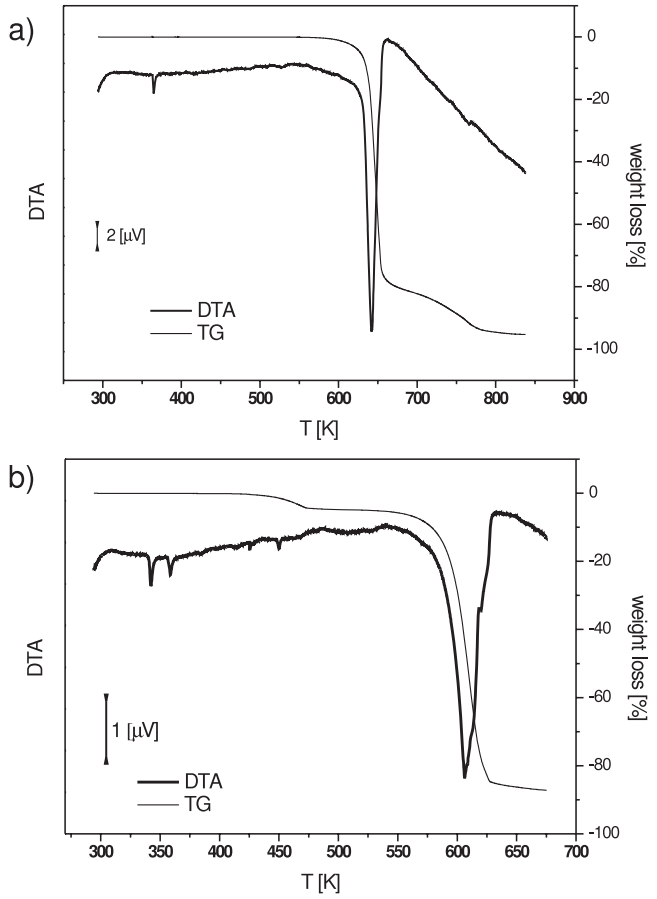

Figure 1. Thermogravimetric analysis and differential thermal analysis scan (with the ramp rate of 2 K min^{-1}, sample mass 12 mg) for the $Gu_3Bi_2I_9$ (a) and $Gu_3Sb_2I_9$ (b) crystals.

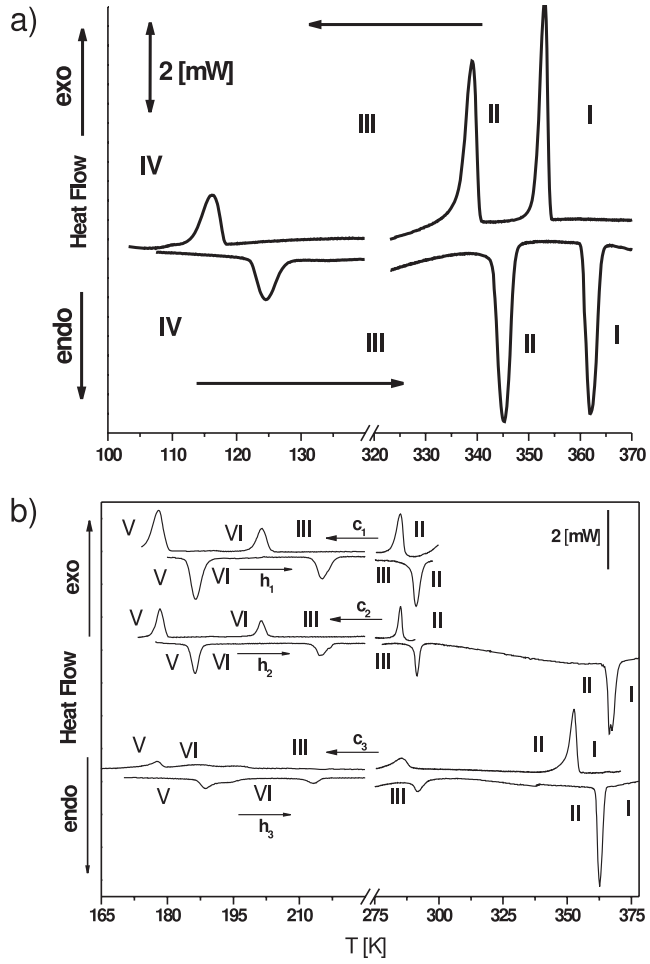

Figure 2. DSC runs (on cooling and heating) for (a) $Gu_3Sb_2I_9$ (DSC with the ramp rate of 10 K min^{-1}, sample mass 15 mg) and (b) $Gu_3Bi_2I_9$ (DSC with the ramp rate of 10 K min^{-1}, sample mass 14 mg) crystals.

cooling scans as well (not shown in figure 3(a)). It is characteristic that at both transitions the dimension of the crystal along the $[\bar{1}10]$ direction diminishes, whereas along the [001] and $[\bar{1}10]$ directions it increases. The dilatometric measurements could be performed for the $Gu_3Bi_2I_9$ sample exclusively perpendicular to the natural plates of the single crystal as grown—[001]. The plates are very thin (below 0.3 mm) and mechanically hard to prepare for measurements. Figure 3(b) shows the dilatometric results obtained in the temperature range corresponding to the 214, 192, 291 and 368 K phase transitions (on heating). The runs, reproducible on heating and cooling, indicate a discontinuous phase transition with a well observed temperature hysteresis. The jump in the $\Delta L/L_0$ value, observed at the 368 K phase transition, is about 0.16, which is unexpectedly large.

3.2. Single-crystal x-ray diffraction results

The x-ray measurements have been performed for the single crystals of $Gu_3Sb_2I_9$ and $Gu_3Bi_2I_9$ at 295, 348 and 364 K. For the antimony analog the determination of the structure was satisfactory at all three temperatures whereas for the bismuth one it was possible merely at 295 K. During structural phase transitions both crystals reveal significant deformation, which is moreover accompanied by the appearance of the ferroelastic structure. The effects mentioned above worsened the quality of the single crystals, i.e. both mechanical defects and mosaic structure increase. The high value of R factors excluded the detailed analysis of the $Gu_3Bi_2I_9$ structure at 348 and 364 K. Nevertheless, the preliminary structural results for $Gu_3Bi_2I_9$ indicate that these iodine compounds are isomorphic in phases I, II and III.

The structure of both compounds is characterized by the layer framework (see figure 4). The layered character of the crystal structures of $Gu_3M_2I_9$ is preserved in all phases for which the x-ray measurements were performed. The essential changes occurring during phase transitions consist in the reorganization of the structural motif within the layers. Two mutually overlapping frameworks, anionic and cationic, may be distinguished in the structure of each layer. The anionic framework consists of the $M_2I_9^{3-}$ face-sharing bioctahedra. In all phases two symmetrically independent types of guanidinium cations (A and B) may be distinguished. They differ in their surroundings and in consequence in the magnitude of the interaction force with the anionic substructure. The structural motif forming the layer structure is presented in figure 5. The guanidinium cations of A type

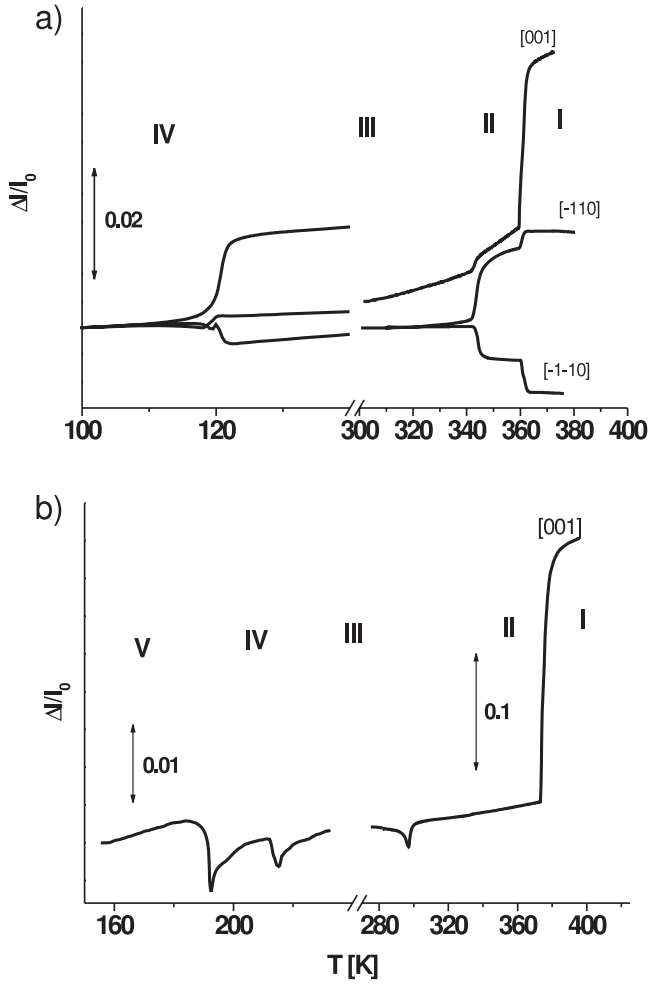

Figure 3. (a) Temperature dependence of the linear thermal expansion, $\Delta L/L_0$, measured along the [001], [$\bar{1}$10] and [$\bar{1}\bar{1}$0] directions (orthorhombic system, phase III, 300 K) at a ramp rate 4 K min^{-1} for $Gu_3Sb_2I_9$ and (b) for $Gu_3Bi_2I_9$ perpendicular to the plate of the crystal as grown.

lie in the middle of the layer structure and they form hydrogen bonds with the bridging iodine atoms of the $M_2I_9^{3-}$ bioctahedra. The cations of B type lie at both edges of the layer at the level of the terminal iodine atoms. In the subsequent phases the mutual orientation of the cations of types A and B changes. The basic unit of the cation framework is composed by three cations arranged in the characteristic way. Due to isomorphism of both iodide derivatives the detailed description of the crystal structure in phases I, II and III is presented for $Gu_3Sb_2I_9$, for which the crystallographic results were of better quality than the bismuth analog.

3.2.1. Structure at 364 K. The x-ray measurements were performed after heating a sample. The structure of $Gu_3Sb_2I_9$ at 364 K was solved and refined in the hexagonal space group $P6_3/mmc$. The enhanced values of the displacement parameters of the carbon and nitrogen atoms indicate a high disorder of the guanidinium cations. The large value of the R factors may be a result of the fact that the crystal has already undergone two successive ferroelastic phase transitions connected with a large distortion of the crystal lattice. The anionic bioctahedral moieties are surrounded by the guanidinium cations arranged in the characteristic triplets. The bond lengths and the angle values for the guanidinium cations are typical of similar structures reported in the literature [20–24]. As expected, the terminal bonds Sb–I (2.871 Å) are shorter than the bridging ones (3.244 Å) (see table 2). Such bond lengths are characteristic of the antimony(III) iodide. The guanidinium cations are placed on the symmetry planes, which are mutually parallel. The cations of type B lie one over the other at a distance of about 7 Å and they form hydrogen bonds with the terminal iodine atom of the $Sb_2I_9^{3-}$ units. In the middle of the distance between them the cation of type A is placed. The distance between the centers of gravity of the B and A cations is equal to about 5.3 Å.

3.2.2. Structure at 348 K. At the I → II phase transition the $Gu_3Sb_2I_9$ crystal passes from the hexagonal to the orthorhombic system. On the basis of the systematic absences the space group $Cmcm$ has been chosen, in which the structure was solved and refined. The change in the crystal system between 364 and 348 K, from hexagonal to orthorhombic, confirmed our optical observation that we deal with the ferroelastic phase transition within this temperature region. The geometry of the $Sb_2I_9^{3-}$ bioctahedron yields insignificant distortion as compared to that in phase I. The terminal Sb–I bond lengths are practically the same and equal to 2.871 and 2.870 Å, whereas the bridging ones are 3.251 and 3.218 Å. The geometry of the guanidinium cations is not deformed essentially; this mutual space arrangement, however, changes. The A cations are still placed inside the layer, in the middle of its thickness. The cations of type B, however, lean out of the plane of the layer and form an angle of 36° one with each other. The centers of gravity of the cations of type A and B are distanced one from each other by 4.5 Å. The displacement parameters of the carbon and nitrogen atoms decrease, which indicates the ordering of the guanidinium cations. While in phase I the free rotation in the plane perpendicular to the threefold axis of the cation is postulated, in phase II the three-site model is more probable. The lattice parameters versus temperature between 300 and 415 K of the $Gu_3Bi_2I_9$ crystal obtained from the x-ray measurements are displayed in figure 6. The lattice parameters are presented in the orthorhombic symmetry. Over phase II the lattice parameters a and b are characterized by opposite temperature coefficients. In the high temperature phase I the dimensions of the unit cell weakly change with temperature. It is clearly seen that the phase transition is accompanied by rapid and huge changes in the unit cell dimensions by about 10%, which is also observed in the dilatometric measurements.

3.2.3. Structure at 295 K. At 295 K the structure was solved in the orthorhombic space group $Cmcm$. This is why the II → III phase transition is regarded as an isostructural one. The structure in phase III may be also solved in the polar space group $Cmc2_1$. The attempt of the structure refinement did not improve the results. The values of the R factors as well as differential maps were comparable to those obtained

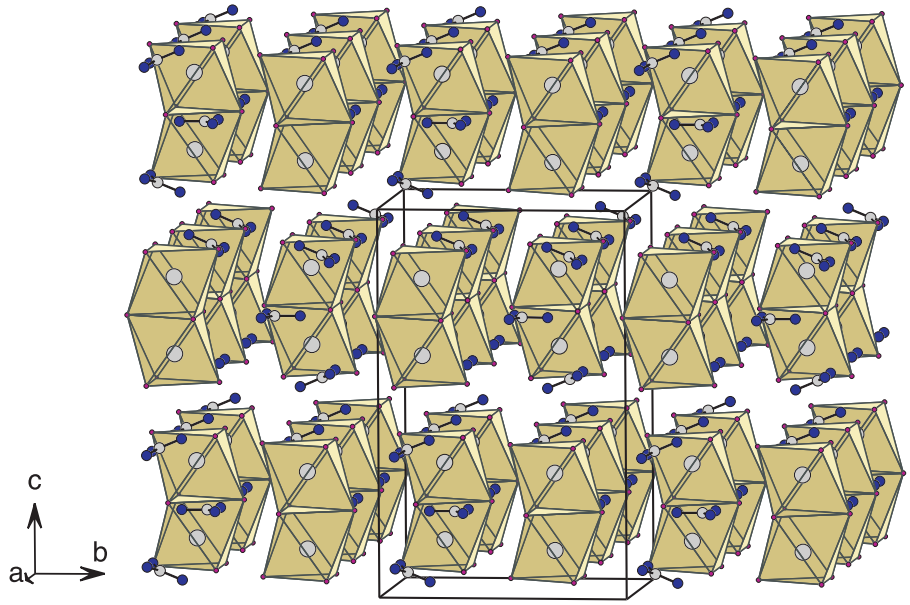

Figure 4. The layer structure of $Gu_3Sb_2I_9$ in phase III. Sb_2I_9 is presented in bioctahedral representation.

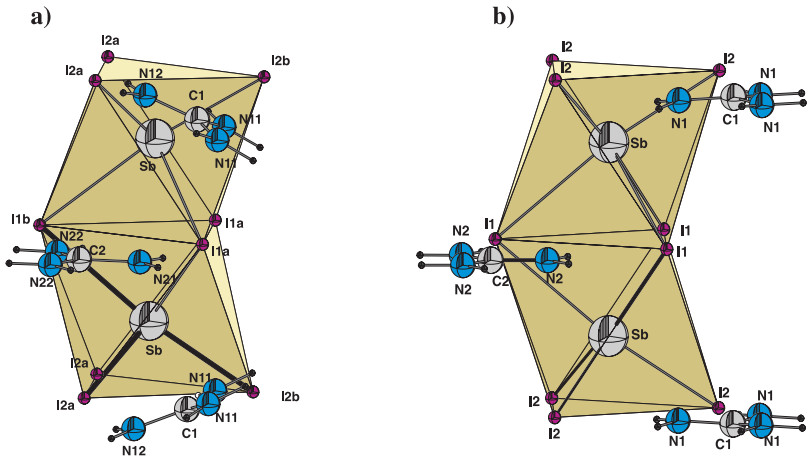

Figure 5. The structural motif forming the layer structure of the $Gu_3Sb_2I_9$ in phase I (a) and III (b).

for the centrosymmetric structure. The presence of the essential correlations between the refined parameters related to each other by a pseudo-center of symmetry decided the final refinement of the structure in the centrosymmetric space group. The pyroelectric measurements, performed above room temperature, did not detect any changes of the pyroelectric current in the vicinity of the II $\rightarrow$ III phase transition. This fact supports the correctness of the choice of the centrosymmetric space group for phase III. The increased compression of the crystal lattice in the subsequent phase transition causes the larger distortion of the $Sb_2I_9^{3-}$ bioctahedra and the change of the mutual arrangement of the guanidinium cations. The terminal Sb–I bond lengths are equal to 2.840 and 2.873 Å, whereas the bridging ones to 3.281 and 3.221 Å. The angle between planes in which the cations of type B are placed increases and is equal to 49°. The centers of gravity of the A and B cations are distanced by about 2.6 Å. The values of the anisotropic temperature factors of the carbon and nitrogen atoms indicate an ordering of the guanidinium cations.

3.3. Dielectric response

The purpose of the dielectric measurements of $Gu_3Sb_2I_9$ was to determine the nature of the phase transitions and to detect the possible motions of the dipolar molecules. The results of measurements of the complex dielectric permittivity, $\epsilon^* = \epsilon' - i\epsilon''$, as a function of temperature and at a frequency of 2 kHz are presented for $Gu_3Sb_2I_9$. The dielectric characteristics of $Gu_3Bi_2I_9$ were not of good quality as a result of the fact that the samples were very thin and they exhibited ferroelastic properties, which affected the reproducibility of the dielectric results. The temperature dependence of the real part of the electric permittivity, ϵ', along the c-axis (orthorhombic system, phase II) is presented in figure 7. The possible motion of the non-dipolar symmetric guanidinium cation (C_{3h}) is not, however, expected to be dielectrically active. Nevertheless,

Table 2. Selected bond lengths [Å] and angles [deg] for $[C(NH_2)_3]_3[Sb_2I_9]$ in phases I, II and III.

Distance		Angle			
		Phase I			
Sb–I1	3.2438(13)	I1–Sb–I1[a]	83.44(1)	N1–C1–N1[g]	119.67(18)
Sb–I1[a]	3.2438(13)	I1–Sb–I1[b]	83.44(1)	N1–C1–N1[h]	119.67(18)
Sb–I1[b]	3.2438(13)	I1[a]–Sb–I1[b]	83.44(1)	N1[g]–C1–N1[h]	119.67(18)
Sb–I2	2.8718(15)	I2–Sb–I2[a]	94.02(5)	N2–C2–N2[i]	120.00(2)
Sb–I2[a]	2.8718(15)	I2–Sb–I2[b]	94.02(5)	N2–C2–N2[j]	120.00(2)
Sb–I2[b]	2.8718(15)	I2[a]–Sb–I2[b]	94.02(5)	N2[i]–C2–N2[j]	120.00(2)
C1–N1	1.206(11)	I1–Sb–I2	91.04(3)		
C1–N1[g]	1.206(11)	I1–Sb–I2	91.04(3)		
C1–N1[h]	1.206(11)	I1–Sb–I2	91.04(3)		
C2–N2	1.249(14)	Sb–I1–Sb[c]	79.58(4)		
C2–N2[i]	1.249(14)	Sb–I1[a]–Sb[c]	79.58(4)		
C2–N2[j]	1.249(14)	Sb–I1[a]–Sb[c]	79.58(4)		
		Phase II			
Sb–I1a	3.2181(8)	I1a–Sb–I1a[d]	82.78(1)	N11–C1–N12	112.1(4)
Sb–I1a[d]	3.2181(8)	I1a–Sb–I1b	84.15(1)	N11–C1–N11[e]	133.6(9)
Sb–I1b	3.2506(14)	I1a[d]–Sb–I1b	84.15(1)	N12–C1–N11[e]	112.1(4)
Sb–I2a	2.8711(8)	I2a–Sb–I2a[e]	93.62(1)	N22–C2–N21	105.7(6)
Sb–I2a[e]	2.8711(8)	I2a–Sb–I2b	94.40(1)	N22–C2–N22[d]	148.6(12)
Sb–I2b	2.8720(11)	I2a[e]–Sb–I2b	94.40(1)	N22[d]–C2–N21	105.7(6)
C1–N11	1.147(6)	I1a–Sb–I2a	91.45(2)		
C1–N11[e]	1.147(6)	I1b–Sb–I2a	89.29(1)		
C1–N12	1.366(8)	I1a–Sb–I2b	91.45(2)		
C2–N22	1.141(7)	I1a–Sb–I2b	91.80(1)		
C2–N22[d]	1.141(7)	Sb–I1a–Sb[d]	79.54(1)		
C2–N21	1.371(10)	Sb–I1a–Sb[d]	79.54(1)		
		Sb–I1b–Sb[d]	78.59(2)		
		Phase III			
Sb–I1a	3.2210(7)	I1a–Sb–I1a[f]	81.34(1)	N11–C1–N12	118.4(5)
Sb–I1a[f]	3.2210(7)	I1a–Sb–I1b	84.29(1)	N11–C1–N11[k]	122.9(9)
Sb–I1b	3.2810(10)	I1a[f]–Sb–I1b	84.29(1)	N12–C1–N11[k]	118.4(5)
Sb–I2a	2.8779(7)	I2a–Sb–I2a[m]	92.37(1)	N22–C2–N21	116.7(8)
Sb–I2a[m]	2.8779(7)	I2a–Sb–I2b	95.21(2)	N22–C2–N22[l]	126.6(16)
Sb–I2b	2.8397(9)	I2a[m]–Sb–I2b	95.21(2)	N22[l]–C2–N21	116.7(8)
C1–N11	1.292(7)	I1a–Sb–I2a	89.29(1)		
C1–N11[k]	1.292(7)	I1b–Sb–I2a	91.45(2)		
C1–N12	1.299(12)	I1a–Sb–I2b	91.80(1)		
C2–N22	1.269(12)	I1a–Sb–I2b	91.47(2)		
C2–N22[l]	1.269(12)	Sb–I1a–Sb[f]	80.33(1)		
C2–N21	1.376(19)	Sb–I1a–Sb[f]	80.33(1)		
		Sb–I1b–Sb[f]	78.56(1)		

Symmetry codes: [a] $1-y, x-y, z$; [b] $1-y+x, 1-x, z$; [c] $1-y, 1-x, 0.5-z$; [d] $1-x, y, 1.5-z$; [e] $1-x, y, z$; [f] $1-x, y, 0.5-z$; [g] $1-y, 1+x-y, z$; [h] $-x+y, 1-x, z$; [i] $1-y, -1+x-y, z$; [j] $2-x+y, 1-x, z$; [k] $-x, y, z$; [l] $2-x, y, 0.5-z$; [m] $1-x, y, 0.5-z$.

some changes in the permittivity value are observed at the phase transition. It seems that this subtle dielectric anomaly should be assigned to the mechanism of the displacive type. Over phase II a rise of ϵ' is observed, which is accompanied by a slight diminishing of the dielectric loss value (not shown in the figure). This may be connected with the appearance of the electric conductivity, which is usually observed in halogenoantimonates(III) or halogenobismuthates(III) at high temperatures. The low temperature phase transition at 120 K is manifested by an almost step-wise decrease of ϵ', which is accompanied by a small value of ϵ''. This effect may be related to some freezing of molecular motion on crossing this phase transition.

3.4. Domains and domain boundaries in the Cmcm phases

The space groups of the isomorphous phases II and III of both compounds and the space group of their high temperature phase I are in a group–subgroup relation $P6_3/mmc \supset Cmcm$ ($D_{6h}^4 \supset D_{2h}^{17}$), which allows one to analyze the phase transition I → II within the Landau theory. The Landau approach is all the more justified because the crystal does not crack and the resulting domains present apparently coherent boundaries in spite of a large transformation strain.

The number of atoms Z per primitive unit cell (but not per conventional centered unit cell of the orthorhombic group) being equal in both phases, the primary order parameter has its

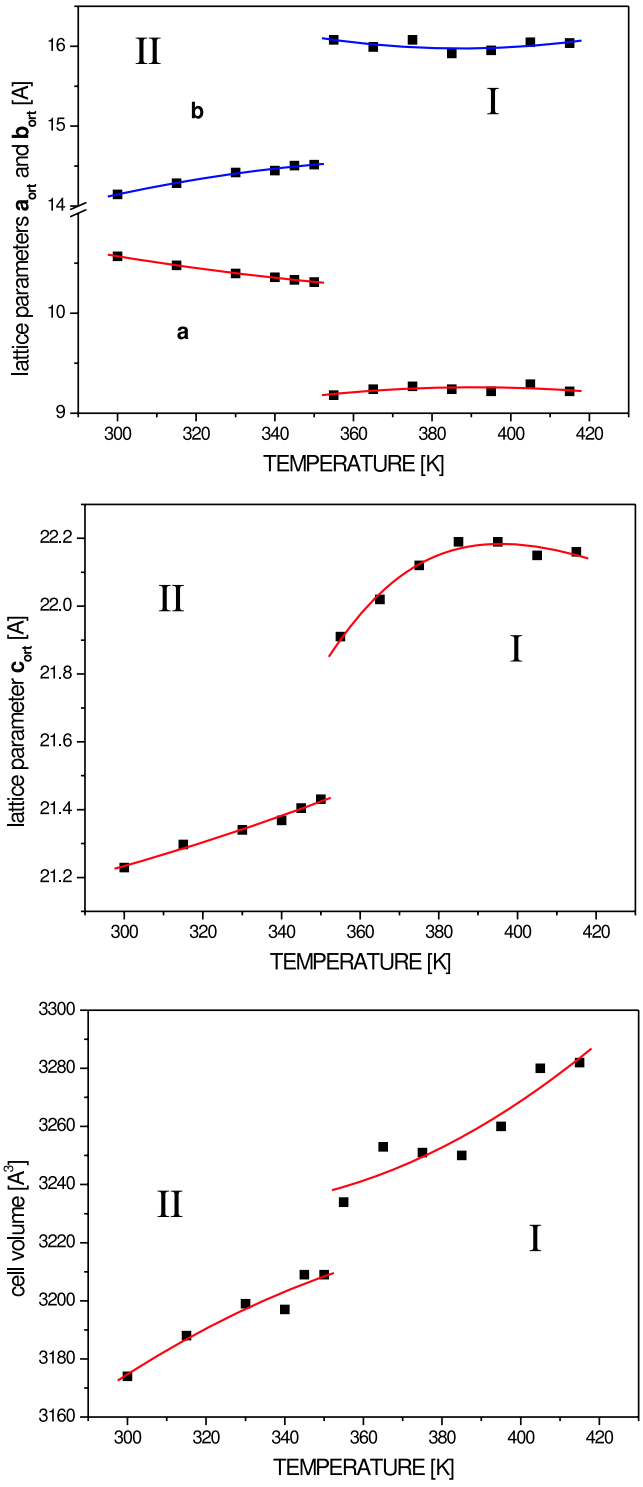

Figure 6. The unit cell parameters of $Gu_3Bi_2I_9$ above room temperature.

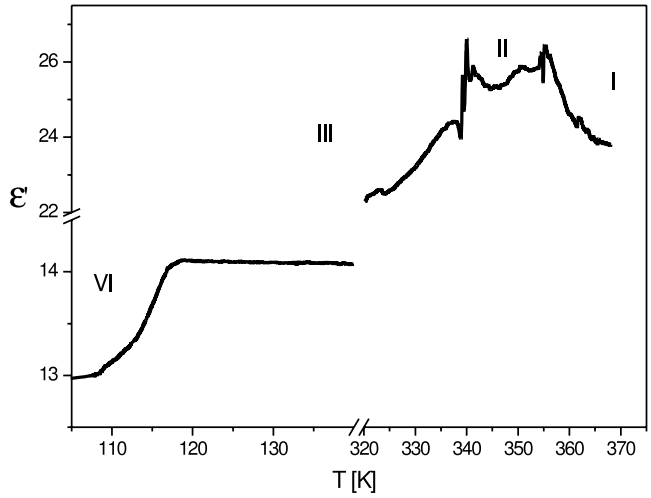

Figure 7. The temperature dependence of the real part of the complex electric permittivity ϵ', for $Gu_3Sb_2I_9$ along the c-axis measured at the frequency of 2 kHz.

wavevector at the Brillouin zone center $k = 0$ so that the low symmetry phase is a proper ferroic. The active representation is equivalent to the 2D irreducible representation E_g of the point group $6/mmm$ (D_{6h}), or in the notation of Kovalev [33]

$$P6_3/mmc \rightarrow (k_{16}, \hat{t}^9) \rightarrow Cmcm. \qquad (1)$$

Because the inversion is preserved in the low symmetry phase, the lowest physical order parameter is strain, so the phase transition belongs to the proper ferroelastic species of Aizu [34].

The spatial orientations of three ferroelastic domains V_I, V_{II} and V_{III} of phase III considered as a result of symmetry reduction are shown in figure 9. The decomposition of the group $P6_3/mmc$ into left cosets of the subgroup $Cmcm$ shows that the lowest symmetry operation relating each pair of variants V_I, V_{II} and V_{III} is a mirror plane m. Therefore, the domains are mirror twins [35]. The mirror planes, being the W stress free domain walls [36], are indicated in figure 9 by thick solid lines. The stress free W′ domain walls are perpendicular to the corresponding W domain walls if the transformation strain is infinitesimally small. When the low symmetry phase deforms with respect to the hexagonal one, the angles between the stress free walls change. In particular the angle between the W and W′ walls separating the same variants, e.g. I and II becomes

$$(\mathrm{W}'_{\mathrm{I-II}}, \mathrm{W}_{\mathrm{I-II}}) = \arctan\left(\frac{b_{\mathrm{ort}}}{a_{\mathrm{ort}}}\right) + \arctan\left(\frac{b_{\mathrm{ort}}}{3a_{\mathrm{ort}}}\right) \qquad (2)$$

where a_{ort} and b_{ort} are lattice constants in the orthorhombic phase perpendicular to the hexagonal axis.

The angle between the W walls separating one selected variant from the remaining two, e.g. I from II and III, is

$$(\mathrm{W}_{\mathrm{I-II}}, \mathrm{W}_{\mathrm{III-I}}) = \frac{\pi}{2} - \arctan\left(\frac{b_{\mathrm{ort}}}{3a_{\mathrm{ort}}}\right). \qquad (3)$$

The angle between the walls of the same variants separated by W′ boundaries is

$$(\mathrm{W}'_{\mathrm{I-II}}, \mathrm{W}'_{\mathrm{III-I}}) = 2\arctan\left(\frac{a_{\mathrm{ort}}}{b_{\mathrm{ort}}}\right). \qquad (4)$$

In the initial phase the ratio $b_{\mathrm{ort}}/a_{\mathrm{ort}} = \sqrt{3}$, and consequently the angles are

$$(\mathrm{W}'_{\mathrm{hexI-II}}, \mathrm{W}_{\mathrm{hexI-II}}) = \frac{\pi}{2} \qquad (5)$$

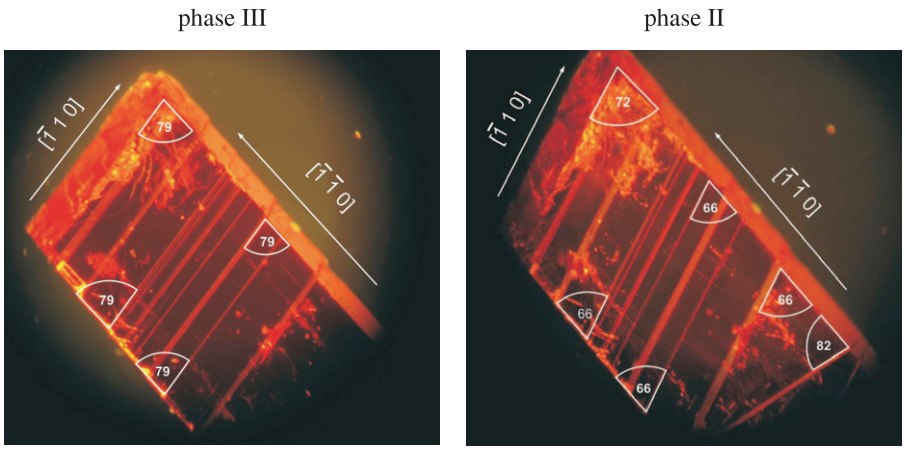

Figure 8. The ferroelastic domain structure of $Gu_3Sb_2I_9$ in phase II and III.

$$(W_{hexI-II}, W_{hexIII-I}) = \frac{\pi}{6} \tag{6}$$

$$(W'_{hexI-II}, W'_{hexIII-I}) = \frac{\pi}{6}. \tag{7}$$

Using the data from table 1 concerning the intermediate phase II, $a = 10.002$ Å and $b = 15.002$ Å, one finds the corresponding angles:

$$(W'_{interI-II}, W_{interI-II}) = 82.89° \tag{8}$$

$$(W_{interI-II}, W_{interIII-I}) = 63.42° \tag{9}$$

and

$$(W'_{interI-II}, W'_{interIII-I}) = 67.65°. \tag{10}$$

The data concerning the room temperature phase III, $a = 11.1079$ Å and $b = 13.3635$ Å, give

$$(W'_{roomI-II}, W_{roomI-II}) = 72.11° \tag{11}$$

$$(W_{roomI-II}, W_{roomIII-I}) = 68.15° \tag{12}$$

and

$$(W'_{roomI-II}, W'_{roomIII-I}) = 79.46°. \tag{13}$$

A simple inspection of figure 9 shows that the angle (W'_{I-II}, W_{I-II}) decreases, whereas (W_{I-II}, W_{III-I}) and (W'_{I-II}, W'_{III-I}) increase with increasing strain, i.e. with decreasing temperature. The experimental macroscopic angles visible in figure 8 are in a very good agreement with these geometrical microscopic predictions if we identify the 66° angles with $(W'_{interI-II}, W'_{interIII-I})$ (equation (10)), the 82° angles with $(W'_{interI-II}, W_{interI-II})$ (equation (8)) in the intermediate phase II and the 79° angles with $(W'_{roomI-II}, W'_{roomIII-I})$ (equation (8)) in the room temperature phase III. The thermal evolutions of the above angles observed under the polarization microscope confirm this identification and, moreover, comply with the temperature dependence of the lattice constants depicted in figure 6. The domain walls move under external stress.

It is interesting that the W domain walls related to the lost mirror planes [36] are practically absent from the microscope images, whereas the prevailing ones are the W′ walls. This can be explained by looking at figure 9. The W walls are inclined with respect to the high symmetry directions of the lattice at an angle that varies with temperature in such a way that the internal structure of the wall has no periodicity except for particular commensurate values. In contrast to this, a W′ wall separates two rectangles along their common diagonal. Thus, the microscopic structure of the W′ walls shows a temperature independent 2D periodicity, which is not the case for the W walls.

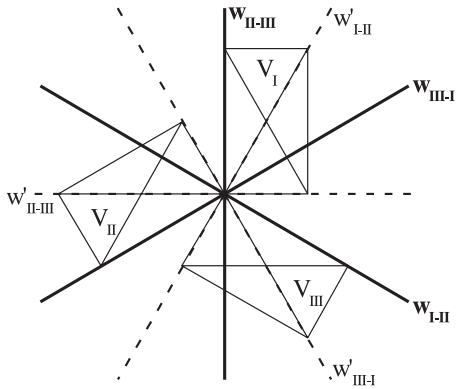

Figure 9. Three variants VI, VII and VIII of phase *Cmcm* as a result of symmetry reduction $P6_3/mmc$. Thick lines and thin dashed lines correspond to W and W′ wall orientation without orthorhombic strain.

4. Discussion

The crystal structures of $Gu_3Sb_2I_9$ and $Gu_3Bi_2I_9$ have been analyzed in various phases of both compounds. The comparison of these structures allows us to propose the molecular mechanism of the ferroelastic phase transition. In the hexagonal high temperature phase (I) of the $Gu_3Sb_2I_9$ crystals the anionic substructure is fully ordered, whereas the cationic one consists of highly orientationally disordered guanidinium moieties. The cations rotate around their threefold axis, which is perpendicular to the molecular plane, by an angle of 120°. This is consistent with the structural

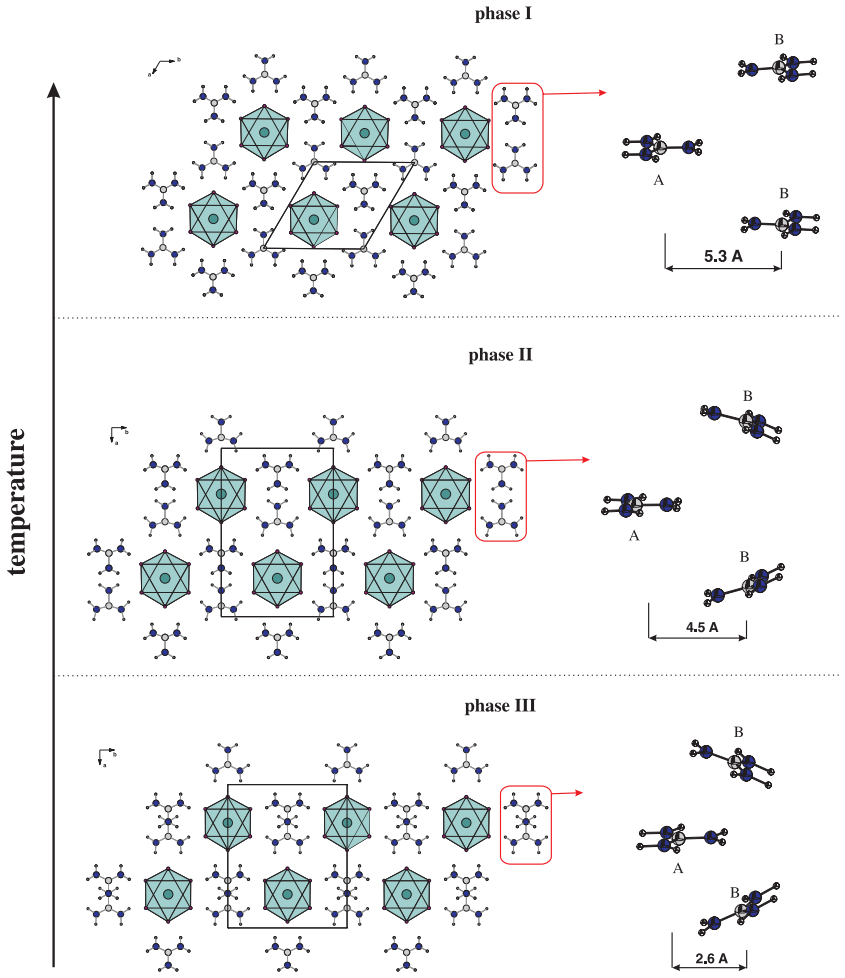

Figure 10. Evolution of the structure of the selected layer during the phase transitions in $Gu_3Sb_2I_9$.

results as well as with the thermodynamic analysis. The characteristic feature of this crystal structure is that the packing of the molecules favors their rearrangement merely within the layer, but this two-dimensional structure remains the same during all the phase transitions. Such a difference of the molecular regrouping manifests itself as anisotropy of a distortion of the crystal lattice during the successive phase transitions. The phase transition I $\rightarrow$ II is connected with lowering of symmetry of the crystal from hexagonal to orthorhombic. Such a change of symmetry requires a rearrangement of the molecules within each layer. The rearrangement is realized in such a way that the anionic framework compresses along the *b*-axis and *c*-axis and expands along the *a*-axis (the notation concerns the orthorhombic phase). This effects result in the significant changes in the mutual positions of the A and B types of cations (see figure 10). The distance between the centers of gravity of both types of cations diminishes along the *b*-axis, which is accompanied by a leaning out of the B type cations toward the *c*-axis (up and down). This effect deepens through the subsequent phase transition (II $\rightarrow$ III). These considerations lead to the conclusion that through the I $\rightarrow$ II phase transition we deal with qualitative changes in the mutual orientations of the cationic planes, whereas for the low temperature phase transition II $\rightarrow$ III these changes are barely of quantitative character (they simply become deeper). This relates mainly to the cations of type B. The ring plane of the cation A in each phase is practically unchanged with regard to its surroundings. This is determined by the steric hindrance and the environment symmetry (i.e. the closest neighbors—iodine atoms). The proposed mechanism of distortion of the crystal lattice on crossing the phase transitions just affects their mechanisms. Basically, two components should be considered in the mechanisms: one of the order–disorder type and the other one of the displacive type. The former mechanism is described above. The displacement of the anionic with respect to cationic framework was directly confirmed in the structural analysis. In turn, the order–disorder mechanism of the phase transition corresponds to the results obtained by the calorimetric studies, which are discussed below. The studies of the thermal properties of $Gu_3Sb_2I_9$ and $Gu_3Bi_2I_9$ over a wide temperature range disclosed quite a complex phase situation. $Gu_3Sb_2I_9$ undergoes three structural phase transitions, at 119/121, 341/344 and 355/362 K (on cooling/heating), and $Gu_3Bi_2I_9$ four transitions, at 184/192, 206/214, 291/295 and 358/368 K; all of them are of the first order type. The magnitude of the transition entropy (ΔS_{tr}) accompanying the phase transition is one of the parameters which allows

us to distinguish between 'order–disorder' and 'displacive' mechanisms. Pure 'displacive' and 'order–disorder' transitions are characterized by ΔS_{tr} values smaller than about 0.5–1 J K^{-1} mol^{-1} and larger than 5.76 J K^{-1} mol^{-1} (R ln 2), respectively. In the case of the guanidinium analogs we should take into account the number of cations contributing to the phase transition mechanism. The transition entropy values, ΔS_{tr}, accompanying the phase transitions in the antimony analog are quite large, being of the order of 12–19 J K^{-1} mol^{-1}. In turn, ΔS_{tr} for the bismuth analog ranges from 4 to 18 J K^{-1} mol^{-1}. It should be noted that the value of the entropy effects found corresponds to the changes in dynamics of at least two guanidinium cations per mole (the ratio of the non-equivalent cations B:A is 2:1). Assuming that two or three cations contribute simultaneously to the mechanism of the phase transition, the entropy effect per cation is equal to about 4–9 J K^{-1} mol^{-1}. This value indicates that the entropy effect is mainly due to the order–disorder contribution of a few molecules. Taking into account the fact that the guanidinium cation is smaller in size and in inertia moment in comparison to the bioctahedral anion, most probably these are the cationic moieties to be orientationally disordered. It should be stressed that this is consistent with our structural results. Such a situation is encountered in the plastic phases of some molecular crystals [25]. The large orientational disorder of molecules is also characteristic of various salts containing methyl-substituted ammonium cations with simple monovalent inorganic anions such as ClO_4^- [26], NO_3^- [27], BF_4^- [28] and SCN^- [29] and in the compounds containing symmetric bulky cations—piperidinium [30], pyrrolidinium [31] and trimethylammonium [32]—and the analogous inorganic anions. It should be noted that the shape of the dielectric function, $\epsilon(T)$ (see figure 7), in the vicinity of the II → I phase transition of $Gu_3Sb_2I_9$ does not, however, resemble those encountered for the crystals with the typical plastic phases. It should be remembered that the guanidinium cations bestow relatively small electric dipole moment (even in the case of distorted cations), which is why releasing their C_3-type motions does not lead to any changes in the dielectric polarizability and subsequently in their increment ($\Delta\epsilon$) observed. Our structural analysis has indicated two possible contributions to the phase transition mechanism: order–disorder and displacive. In spite of the fact that these two contributions participate in the mechanism of the high temperature phase transitions, the motion of the symmetric (non-dipolar) cations is undoubtedly inactive in dielectric spectroscopy. In our opinion the dielectric anomalies, observed either at the III → II or at the II → I phase transition, are most probably determined by the displacive mechanism of the transitions.

5. Conclusions

(i) The crystal structure of $Gu_3Sb_2I_9$ and $Gu_3Bi_2I_9$ is built up of discrete bioctahedral anionic units ($M_2I_9^{3-}$) and two kinds of non-equivalent guanidinium cations. The title crystals at room temperature crystallize in the orthorhombic space group— $Cmcm$, whereas the highest temperature transformation leads to the prototypic phase (paraelastic) of hexagonal symmetry $P6_3/mmc$.

(ii) Both guanidinium analogs reveal a rich polymorphism. The $Gu_3Sb_2I_9$ crystal undergoes three structural phase transitions of first order type, at 119/121, 341/344 and 355/362 K (cooling/heating), whereas $Gu_3Bi_2I_9$ four transitions, at 184/192, 206/214, 291/295 and 358/368 K.

(iii) Both crystals reveal the ferroelastic domains below 362 K (Sb) and 368 K (Bi), respectively.

(iv) The mechanism of the paraelastic–ferroelastic phase transition is complex. The contribution of the mechanism of both the order–disorder and displacive types is confirmed. The former contribution is related to the reorientational disorder of the guanidinium cations, the latter one to the mutual shift of the anionic and cationic frameworks.

(v) The most striking property of the crystals under study is that they show an enormous plasticity that prevents them from cracking when undergoing phase transitions that involve rather strong spontaneous strains. Additionally, the mobility of the domain structure under external stress makes them similar to metallic crystals, especially undergoing the martensitic phase transitions. The reason for this hyperplasticity may be related to a system of hydrogen bonds. This point is worth further studies as it may initiate a search for molecular crystalline materials showing e.g. a shape memory effect.

Acknowledgment

This work was supported by the Polish State Committee for Research (project register number N N202 1050 33).

References

[1] Jakubas R and Sobczyk L 1990 *Phase Transit.* **20** 163
[2] Varma V, Bhattacharjee R, Vasan H N and Rao C N R 1992 *Spectrochim. Acta* A **48** 1631
[3] Sobczyk L, Jakubas R and Zaleski J 1997 *Pol. J. Chem.* **71** 265 and references cited therein
[4] Jakubas R, Krzewska U, Bator G and Sobczyk L 1988 *Ferroelectrics* **77** 129
[5] Zaleski J and Pietraszko A 1996 *Acta Crystallogr.* B **52** 287
[6] Kawai T, Takao E, Shimanuki S, Iwata M, Miyashita A and Ishibashi Y 1999 *J. Phys. Soc. Japan* **68** 2848
[7] Jakubas R 1989 *Solid State Commun.* **69** 267
[8] Lefebvre J, Carpentier P and Jakubas R 1995 *Acta Crystallogr.* B **51** 167
[9] Józków J, Bator G, Jakubas R and Pietraszko A 2001 *J. Chem. Phys.* **114** 7239
[10] Kuok M H, Ng S G, Tan I S, Rang Z I, Iwata M and Ishibasi Y 1998 *Solid State Commun.* **108** 159
[11] Jakubas R, Piecha A, Pietraszko A and Bator G 2005 *Phys. Rev.* B **72** 104107
[12] Bator G, Zeegers-Huyskens T H, Jakubas R and Zaleski J 2001 *J. Mol. Struct.* **570** 61
[13] Szklarz P, Zaleski J, Jakubas R, Bator G, Medycki W and Faliska K 2005 *J. Phys.: Condens. Matter* **17** 2509
[14] Zaleski J and Pietraszko A 1994 *J. Mol. Struct.* **327** 287
[15] Jakubas R, Zaleski J, Kosturek B and Bator G 1999 *J. Phys.: Condens. Matter* **24** 4731
[16] Oxford Diffraction 2001 CrysAlis 'CCD' and CrysAlis 'RED', Oxford Diffraction (Poland) Sp. z o.o, Wrocaw, Poland

[17] KUMA 1996 KUMA Diffraction Software. Version 8.1.0 and 8.1.1, KUMA Diffraction, Wrocaw, Poland
[18] Sheldrick G M and SHELX-97 1997 Program for solution and refinement of crystal structure, University of Göttingen Germany
[19] Sheldrick G M 1990 SHELXTL *Siemens Analytical X-ray Instruments Inc.* Madison, Wisconsin, USA
[20] Carmalt C J, Farrugia L J and Norman N C 1995 *Z. Anorg. Allg. Chem.* **621** 47
[21] Carmalt C J, Farrugia L J and Norman N 1994 *Polyhedron* **13** 1655
[22] Chaabouni S, Kamoun S and Jaud J 1997 *J. Chem. Cryst.* **27** 527
[23] Harrison W T A 2003 *Acta Crystallogr.* E **59** o769
[24] Harrison W T A and Phillips M L F 1997 *Chem. Mater.* **9** 1837
[25] Sherwood J N 1979 *The Plastically Crystalline State* (New York: Wiley)
[26] Ishida H, Ikeda R and Nakamura D 1987 *Bull. Chem. Soc. Japan.* **60** 467
[27] Ishida H, Ikeda R and Nakamura D 1985 *J. Chem. Soc. Faraday Trans.* **281** 963
[28] Ishida H, Hayama N and Ikeda R 1992 *Chem Lett.* **1333**
[29] Tanabe T, Ikeda R and Nakamura D 1991 *J. Chem. Soc. Faraday Trans.* **87** 987
[30] Ono H, Ishimaru S, Ikeda R and Ishida H 1997 *Chem. Phys. Lett.* **275** 485
[31] Ono H, Ishimaru S, Ikeda R and Ishida H 1999 *Bull. Chem. Soc. Japan* **72** 2049
[32] Kuchitsu K, Ono H, Ishimaru S, Ikeda R and Ishida H 2000 *Phys. Chem. Chem. Phys.* **2** 3883
[33] Kovalev O V 1965 *Irreducible Representations of the Space Groups* (New York: Gordon and Breach)
[34] Aizu K 1970 *Phys. Rev.* B **2** 754
[35] Guymont M 1978 *Phys. Rev.* B **18** 5385
[36] Sapriel J 1975 *Phys. Rev.* B **12** 5128